Magnetic Resonance Characterization of Cardiac Adaptation and Myocardial Fibrosis in Pulmonary Hypertension Secondary to Systemic-To-Pulmonary Shunt

Daniel Pereda, MD*; Inés García-Lunar, MD*; Federico Sierra, BS; Damián Sánchez-Quintana, MD; Evelyn Santiago, MD; Constanza Ballesteros, BS; Juan F. Encalada, MD; Javier Sánchez-González, PhD; Valentín Fuster, MD, PhD; Borja Ibáñez, MD, PhD; Ana García-Álvarez, MD, PhD

Background—Pulmonary hypertension (PH) and right ventricular (RV) dysfunction are strong predictors of morbidity and mortality among patients with congenital heart disease. Early detection of RV involvement may be useful in the management of these patients. We aimed to assess progressive cardiac adaptation and quantify myocardial extracellular volume in an experimental porcine model of PH because of aorto-pulmonary shunt using cardiac magnetic resonance (CMR).

Methods and Results—To characterize serial cardiac adaptation, 12 pigs (aorto-pulmonary shunt [n=6] or sham operation [n=6]) were evaluated monthly with right heart catheterization, CMR, and computed tomography during 4 months, followed by pathology analysis. Extracellular volume by CMR in different myocardial regions was studied in 20 animals (aorto-pulmonary shunt [n=10] or sham operation [n=10]) 3 months after the intervention. All shunted animals developed PH. CMR evidenced progressive RV hypertrophy and dysfunction secondary to increased afterload and left ventricular dilatation secondary to volume overload. Shunt flow by CMR strongly correlated with PH severity, left ventricular end-diastolic pressure, and left ventricular dilatation. T1-mapping sequences demonstrated increased extracellular volume at the RV insertion points, the interventricular septum, and the left ventricular lateral wall, reproducing the pattern of fibrosis found on pathology. Extracellular volume at the RV insertion points strongly correlated with pulmonary hemodynamics and RV dysfunction.

Conclusions—Prolonged systemic-to-pulmonary shunting in growing piglets induces PH with biventricular remodeling and myocardial fibrosis that can be detected and monitored using CMR. These results may be useful for the diagnosis and management of congenital heart disease patients with pulmonary overcirculation. (***Circ Cardiovasc Imaging*. 2016;9:e004566. DOI: 10.1161/CIRCIMAGING.116.004566.**)

Key Words: cardiac magnetic resonance ■ congenital heart disease ■ experimental models ■ pulmonary hypertension ■ T1 mapping

Pulmonary hypertension (PH) is relatively common among patients with congenital heart disease (CHD),[1,2] especially in conditions with pulmonary overcirculation and important volume and pressure overload (eg, large ventricular septal defect, aorto-pulmonary window, patent ductus arteriosus, or palliative arterial shunts). PH and right ventricular (RV) failure are strong predictors of mortality in CHD.[3,4] Over the past decades, advances in pediatric cardiology and surgical techniques have increased the number of patients with CHD surviving into adulthood. However, decision on the optimal treatment or timing of a surgical repair remain challenging in several CHD (like, eg, in the presence of moderate-sized ventricular septal defects in asymptomatic small children). Indication may depend in some instances on PH and RV performance monitoring, which is difficult in this population. Children with PH are at a significantly higher risk of major complications during right heart catheterization (RHC),[5] and echocardiographic evaluation of the RV is complex, particularly in the presence of anatomic alterations.

See Editorial by Grosse-Wortmann
See Clinical Perspective

Received January 11, 2016; accepted July 21, 2016.

From the Centro Nacional de Investigaciones Cardiovasculares Carlos III (CNIC), Madrid, Spain (D.P., I.G.-L., F.S., C.B., V.F., B.I., A.G.-Á.); Hospital Clínic, IDIBAPS, Barcelona, Spain (D.P., E.S., J.F.E., A.G.-Á.); Hospital Universitario Quirón Madrid, UEM, Spain (I.G.-L.); Facultad de Medicina, Universidad de Extremadura, Badajoz, Spain (D.S.-Q.); IIS-Fundación Jiménez Díaz, Madrid, Spain (B.I.); Philips Healthcare, Madrid, Spain (J.S.-G.); and Zena and Michael A. Wiener Cardiovascular Institute, Mount Sinai School of Medicine, New York (V.F.).

*Drs Pereda and García-Lunar contributed equally to this work.

Correspondence to Ana García-Álvarez, MD, PhD, Centro Nacional de Investigaciones Cardiovasculares Carlos III (CNIC), Melchor Fernández Almagro 3, 28029 Madrid, Spain. E-mail ana.garcia@cnic.es; anagarci@clinic.ub.es or Borja Ibañez, MD, PhD, Centro Nacional de Investigaciones Cardiovasculares Carlos III (CNIC), Melchor Fernández Almagro 3, 28029 Madrid, Spain. E-mail bibanez@cnic.es

Circ Cardiovasc Imaging **is available at http://circimaging.ahajournals.org** **DOI: 10.1161/CIRCIMAGING.116.004566**

Cardiac magnetic resonance (CMR) is the gold standard technique for the assessment of ventricular structure, function, and myocardial scarring. Additionally, it allows for accurate measurement of pulmonary-to-systemic flow ratio (Q_p/Q_s) and may be helpful for quantifying and monitoring pulmonary vascular resistance (PVR).[6,7] The presence of late gadolinium enhancement (LGE) in children and young adults with CHD is a prognostic marker.[8–10] In recent years, T1 mapping has emerged as a noninvasive technique for the quantification of myocardial extracellular volume (ECV), holding the promise of early detection of myocardial involvement not detectable by LGE.[11] In contrast to LGE imaging that detects patchy areas of dense scarring, T1 mapping evidences a diffuse fibrotic process. This novel technique has been scarcely used in this scenario.[12]

We hypothesized that CMR may be useful to monitor serial changes in cardiac remodeling and pulmonary hemodynamics and may be able to detect early myocardial fibrosis in a translational animal model of aorto-pulmonary shunt.

The aorto-pulmonary shunt in growing piglets has become a well-established model of congenital conditions with left-to-right shunt.[13,14] Hemodynamic measures taken at 3 and 6 months after surgery and pathobiology description of this swine model have been already published.[13,15,16] However, serial hemodynamic measurements and, more importantly, a comprehensive description of the progressive cardiac structural adaptation to this chronic volume and pressure overload have not been performed yet.

This study had, therefore, 2 main objectives: (1) to describe the CMR serial features of growing piglets with a large aorto-pulmonary shunt and to correlate them with serial data obtained from right RHC and computed tomography (CT); and (2) to quantify myocardial ECV by CMR in different ventricular territories in shunted animals and to evaluate their correlation with hemodynamic variables and cardiac performance.

Methods

Study Design

The study was designed into 2 substudies and included a total of twenty 4-week-old castrated male Large-White pigs.

Substudy 1 aimed to characterize serial cardiac adaptation to pulmonary overcirculation in 12 animals (aorto-pulmonary shunt [n=6] or sham operation [n=6]). Animals were evaluated monthly with RHC, CMR, and CT (all 3 techniques performed consecutively on the same day) during 4 months and underwent pathology analysis at completion.

Substudy 2 aimed to quantify ECV by CMR in different regions of the myocardium 3 months after the intervention in 20 animals (aorto-pulmonary shunt [n=10] or sham operation [n=10]).

Our Institutional Animal Research Committee approved the study protocol. All animals received care in compliance with the *Guide for the Care and Use of Laboratory Animals*. Before any procedure, animals were anesthetized with an intramuscular injection of ketamine (20 mg/kg), xylazine (2 mg/kg), and midazolam (0.5 mg/kg). Buprenorphine (0.3 mg/kg) was used for analgesia, and animals were intubated.

All hemodynamic, CMR, and CT studies were performed under spontaneous ventilation, anesthesia with intravenous midazolam (0.2 mg/kg/h), and continuous electrocardiographic and pulsioxymetric monitoring.

Description of the Surgical Procedure for Aorto-Pulmonary Shunting

Surgery is performed through a 5 cm thoracotomy on the 4th left intercostal space. The pericardium is incised and the pulmonary artery (PA) is mobilized. The left innominate artery is also mobilized, proximally clamped in the aortic arch and ligated and divided as distally as possible. A side-biting clamp is placed in the main PA, and a 5 mm orifice is created. The distal innominate artery is then anastomosed to the main PA in an end-to-side fashion using interrupted polypropylene sutures (Figure 1). Immediately after flow is restored, a continuous thrill inside the PA confirms correct shunt functionality. After appropriate hemostasis, the lung is re-expanded during chest closure, so no drainage is needed. Animals are extubated immediately after the procedure.

Control animals for this study underwent a sham operation as described earlier, in which the innominate artery was divided but the shunt was not performed.

Pigs undergoing shunting received a single dose of furosemide 40 mg EV immediately after surgery and oral aspirin100 mg daily during the first month.

RHC Studies

A femoral Swan-Ganz catheter positioned under fluoroscopy was used to measure pulmonary artery pressure (PAP) and cardiac output (CO) by the thermodilution method. A femoral arterial line was placed for continuous systemic blood pressure monitoring, and a pigtail catheter was placed inside the left ventricular (LV) cavity to measure LV end-diastolic pressure (LVEDP) as an estimate of left atrial pressure. PVR was calculated in Wood units as (mean PAP–LVEDP)/CO. Indexed PVR and CO by body surface area were estimated using the Brody's formula.[17]

CMR Studies

Studies were performed using a 3.0-T TX Achieva system (Philips, the Netherlands). Steady-state free precession cine sequences were acquired in 10 to 15 contiguous short-axis slices covering both ventricles from base to apex for the evaluation of ventricular volumes and function. Two-dimensional flow imaging (phase-contrast) was performed perpendicular to the main PA and ascending aorta with a velocity-encoded gradient echo sequence, as previously described.[7] In shunted animals, additional phase-contrast transversal imaging of the shunt was performed.

At third month postintervention, CMR imaging protocol included LGE and T1 mapping sequences in all cases. Gadolinium contrast (Magnevist; Bayer Schering Pharma) was administered at a dose of 0.1 mmol/kg for LGE sequence acquired after 15 minutes as recommended by guidelines[18] and followed by 0.0011 mmol/kg/min for a 20-minute infusion for equilibrium contrast imaging, with a cumulative contrast dose of 0.122 mmol/kg. The T1-mapping sequence (Modified Look-Locker Inversion recovery [MOLLI]) was acquired just before contrast administration and after equilibrium in a short-axis view at the level of the papillary muscles, as previously described.[19] All MOLLI sequences were based on a 3 to 5 scheme using a single-shot steady-state free precession readout sequence (TR/TE/α=2.7 ms/1.36 ms/50°) with an in-plane acquisition resolution of 1.2×1.5 mm,^{2} inversion interval of 185 ms, half scan of 0.6, shot duration of 174 ms, and slice thickness of 8 mm. T1 maps were generated by nonlinear fitting of different inversion time points.

Analysis of CMR acquisitions was performed using specialized software (Extended MR Workspace; Philips, The Netherlands) by 2 observers blinded to hemodynamic measurements and histology results. On cine images, biventricular endocardial contours were manually traced in end diastole and end systole, and Simpson's method was used to calculate volumes and ejection fraction. For phase-contrast analysis, the inner contour of the main PA and ascending aorta were outlined in each cardiac phase to quantify the minimum and maximum areas, average velocities, and stroke volumes. Similarly, the inner contours of the shunt were outlined in each cardiac phase to quantify the stroke volume through the shunt. Ventricular volumes and masses and PA areas were adjusted to body surface area. RV–arterial coupling (E_s/E_{max}) was estimated as ([mean PAP– LVEDP]/RV stroke volume index/[mean PAP/

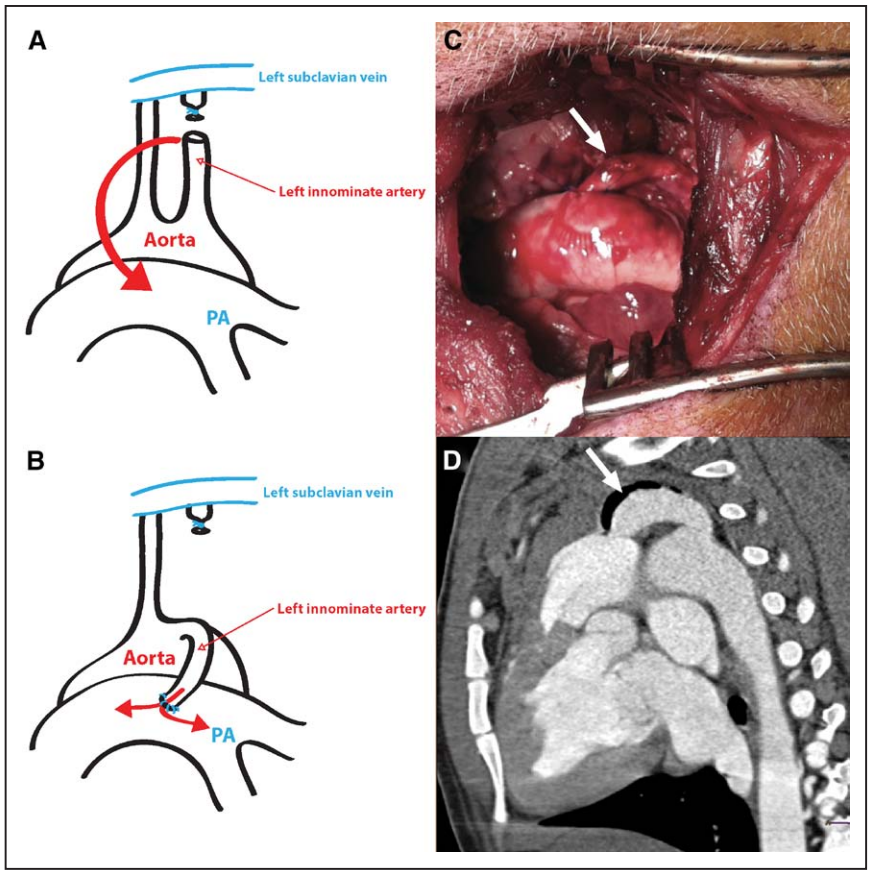

Figure 1. A and **B**, Diagram showing the configuration of the shunt between the left innominate artery and the main PA. **C**, Photograph of the completed procedure after releasing the clamps. **D**, Angio-CT image showing the widely patent shunt 3 months after the procedure. White arrow shows the left innominate artery anastomosed to the main PA. CT indicates computed tomography; and PA, pulmonary artery.

RV end-systolic volume index])[20] using the hemodynamic data registered immediately before the CMR. Regions of interest were drawn on T1 maps in the myocardial RV insertion points, septum, LV lateral wall, and LV cavity blood pool before contrast administration and after equilibrium, as previously shown.[19] T1 mapping images were acquired with high in-plane resolution to facilitate drawing the regions of interest inside the myocardium, and heart rate was updated before every MOLLI acquisition to define the right trigger delay to minimize spatial misregistration. Native T1 values were obtained from precontrast T1 map, and ECV values were calculated as previously described.[21]

CT Studies

CT studies were performed on a monthly basis in shunted animals to confirm permeability of the shunt using a 64-slice scanner (Brilliance Philips) with retrospective electrocardiographic gating. Nonionic iodinated contrast agent (30–40 mL; Isovue 300) was injected through a peripheral vein at a rate of 4 mL/s with a power injector followed by a 30 mL saline flush. A bolus tracking technique was used to appropriately trigger image acquisition once attenuation in the RV reached a preset threshold of 100 HU.

Postprocessing of CT images was performed using dedicated software (Extended Brilliance Workspace 3.5; Philips) and included multiplanar, volume-rendered, and shaded-surface display reconstructions. Shunt maximal orthogonal diameters and cross-sectional area were measured at end-diastole.

Histopathology

Masson's trichrome and picrosirius red stainings were used to evaluate microscopic changes and the presence of collagen using a stereomicroscope provided with digital camera (Nikon SM 1500; Nikon). Quantification of the intimal and medial layer thickness in intraparenchymatous arteries was performed on 20 lung samples (right lower pulmonary lobe) from shunted pigs and compared with 20 samples from sham controls.

Morphometric analysis of the collagen network in the RV insertion points and LV lateral wall was performed in 6 shunted animals and 6 sham-operated controls (15 randomly chosen fields [10× magnification] from each specimen) using picrosirius red staining and dedicated software (SigmaScan Pro 5.0; Jandel Scientific). In each field, a grid of vertical and horizontal lines was used, providing 121 intersection points. The proportion of connective tissue in each specimen, expressed as connective tissue density, was defined as the percentage of intersection points occupied by collagen.

Quantification of cellular and extracellular fractions was performed in the same 12 animals (3 randomly chosen fields from each specimen at 40× magnification) using Masson's trichrome staining and ImageJ (National Institutes of Health; MD) to delineate the corresponding areas.

Statistical Analysis

Continuous variables are expressed as median (interquartile range). Comparisons of continuous variables between groups were performed using Mann–Whitney *U* test. Concordance among CO measured by CMR and thermodilution was assessed with the intraclass correlation coefficient for absolute agreement. Correlations between hemodynamic and CRM parameters were assessed using Pearson or Spearman correlation depending on the association type (linear or curvilinear) evaluated with scatter plots. A P value <0.05 was considered statistically significant. Adjustment for multiple comparisons was not performed. Analyses were performed using SPSS 20 (IBM Corp).

Results

Characterization of the Aorto-Pulmonary Shunt Model

Hemodynamic Data

Hemodynamic data are displayed in Table 1. All animals with aorto-pulmonary shunt developed PH. As compared

Table 1. Hemodynamic Follow-Up Data Obtained by Right and Left Heart Catheterization

	1 Month			2 Months			3 Months			4 Months		
	Shunt (n=6)	Sham (n=6)	*P* Value	Shunt (n=6)	Sham (n=6)	*P* Value	Shunt (n=6)	Sham (n=6)	*P* Value	Shunt (n=6)	Sham (n=6)	*P* Value
Weight, kg	18.0 (13.0–23.0)	27.0 (20.0–28.5)	0.093	34 (29–43.5)	38.5 (37–46.5)	0.180	48.8 (43–57)	54.5 (48–61)	0.310	64.5 (57.5–75)	71.5 (61.5–80)	0.394
BSA, m^2	0.60 (0.49–0.71)	0.78 (0.65–0.80)		0.9 (0.82–1.05)	1.0 (1.0–1.1)		1.1 (1.04–1.25)	1.22 (1.12–1.31)		1.35 (1.26–1.49)	1.45 (1.31–1.58)	
Heart rate, bpm	90.5 (86–92)	84.5 (71–106)	0.485	94.5 (81–103)	84 (83–90)	0.537	88 (82–94)	79.5 (70–88)	0.180	91.5 (80–94)	70.5 (66–72)	0.002
Oxygen saturation, %	92.5 (91–97)	92.5 (90–95)	0.937	91.5 (83–93)	94 (92–96)	0.132	92 (89–95)	97 (94–97)	0.026	90 (89–93)	94.5 (94–98)	0.009
Systolic BP, mm Hg	108.5 (106–113)	108.5 (95–118)	0.662	128 (118–133)	123.5 (117–127)	0.429	125 (125–132)	113.5 (112–126)	0.240	124.5 (124–132.5)	120.5 (110.5–133)	0.589
Diastolic BP, mm Hg	61.0 (59–66)	71.5 (67–79)	0.126	78 (74–78)	85.5 (80–87)	0.126	76.5 (66–81)	82.5 (82–86)	0.093	78 (72–83)	78.5 (70–84)	0.937
Mean BP, mm Hg	80 (77–81)	88 (81–92)	0.247	95 (92–101)	101.5 (94–105)	0.329	94.5 (89–101)	96.5 (95–100)	0.589	97.5 (91–98)	98 (92–106)	0.699
Systolic PAP, mm Hg	33 (30–37)	25.5 (22–31)	0.132	34.5 (34–45)	28 (27–28)	0.009	36.5 (34–42)	29 (25–31)	0.015	45 (40–51)	30.5 (26–33)	0.002
Diastolic PAP, mm Hg	20.5 (18–22)	13 (12–16)	0.004	23 (19–27)	14.5 (13–16)	0.002	22.5 (13–19)	15.5 (13–19)	0.004	28 (24–33)	14.5 (13–15)	0.002
Mean PAP, mm Hg	25.5 (23–27)	19 (14–20)	0.009	28.5 (25–34)	21.5 (20–23)	0.004	28.5 (26–34)	21.5 (18–24)	0.002	34.5 (31–40)	21.5 (20–24)	0.002
RAP, mm Hg	4 (2–7)	2 (2–4)	0.329	2.5 (2–6)	3 (2–4)	0.937	2 (1–5)	2 (0–5)	0.818	3 (2–4)	3 (1–4)	0.699
Cardiac output, L/min	2.2 (1.6–2.6)	3.3 (2.1–4.8)	0.240	4.1 (3.9–4.7)	4.4 (4.0–5.4)	0.394	5.0 (3.7–5.8)	5.4 (5.1–5.6)	0.937	5.5 (4.3–6.1)	6.4 (5.7–6.7)	0.310
Cardiac index, L/min/m^2	3.8 (3.4–4.1)	4.4 (2.9–5.2)	0.699	4.4 (4.00–4.7)	4.8 (4.1–4.9)	0.394	4.5 (3.8–5.8)	4.1 (3.8–4.7)	0.818	3.7 (3.6–4.8)	4.1 (3.5–4.6)	1.000
PWP, mm Hg	10 (8–12)	6.5 (5–7)	0.026	11.0 (8–13)	7.0 (6–9)	0.041	12.0 (10–16)	5 (4–8)	0.015	15 (12–17)	6.5 (3–8)	0.004
LVEDP, mm Hg	10 (10–13)	5.0 (5.0–6.0)	0.009	9.5 (9–13)	8.5 (6–9)	0.065	12 (9–16)	7.5 (6–9)	0.065	15 (15–18)	9 (7–11)	0.002
TPG, mm Hg	14.0 (12.8–16.3)	14.0 (10.5–17.0)	0.792	17.0 (15.5–22.0)	12.5 (11.0–17.3)	0.065	19.0 (15.0–21.5)	15.0 (12.0–15.3)	0.041	18.5 (16.0–24.3)	13.5 (11.3–15.3)	0.004
PVR, WU	6.4 (4.9–9.1)	3.9 (3.4–5.0)	0.132	4.5 (4.1–5.3)	2.8 (2.6–3.3)	0.002	3.8 (2.7–4.3)	2.7 (2.2–2.9)	0.132	3.9 (2.8–4.2)	2.0 (2.0–2.4)	0.009
Indexed PVR, WU m^2	4.0(3.2–4.5)	3.5 (2.7–4.0)	0.310	4.2 (3.5–5.3)	2.9 (2.7–3.4)	0.015	4.5 (3.0–5.2)	3.3 (2.9–3.8)	0.132	4.9 (4.2–5.2)	3.3 (2.6–4.0)	0.026

BP indicates blood pressure; BSA, body surface area; LVEDP, left ventricular end-diastolic pressure; PAP, pulmonary artery pressure; PVR, pulmonary vascular resistance; PWP, pulmonary wedge pressure; RAP, right atrial pressure; and TPG, transpulmonary gradient.

with controls, animals with shunts showed significantly higher mean and diastolic PAP already at 1 month after surgery (Figure 2A). LVEDP and PA wedge pressure were also significantly higher at the first month. Differences in PVR index reached statistical significance at the fourth follow-up visit (Figure 2B). No differences were observed in systemic pressures or cardiac index. Oxygen saturation was significantly lower in shunted animals after the third month, and heart rate was significantly higher in shunted animals only at the last visit.

CMR Data

CMR data are displayed in Table 2. Compared with controls, animals with aorto-pulmonary shunt developed significant RV hypertrophy and dysfunction (increased RV mass from the third month onwards and reduced RV ejection fraction from the second month; Figure 2C). Significant RV–arterial uncoupling was observed in shunted animals from the second month. On the LV, shunted animals showed progressive remodeling with significant dilatation already from the first month (Figure 2D). The main PA was significantly dilated, and PA average flow velocity was reduced from the first month in shunted animals.

The correlation between CO assessed by thermodilution and CMR using different methods in shunted animals was excellent: (1) phase contrast in the PA (intra-class correlation [ICC]=0.895, 95% confidence interval [CI] 0.734–0.957), (2) RV volumetry (ICC=0.961, 95% CI 0.910–0.983), (3) the difference between CO by phase contrast in the aorta and flow through the shunt (ICC=0.813, 95% CI 0.402–0.934), and (4) the difference between CO by LV volumetry and flow through the shunt (ICC=0.948, 95% CI 0.866–0.980). Flow through the shunt showed an excellent concordance with the difference between systemic-to-pulmonary CO as assessed by phase

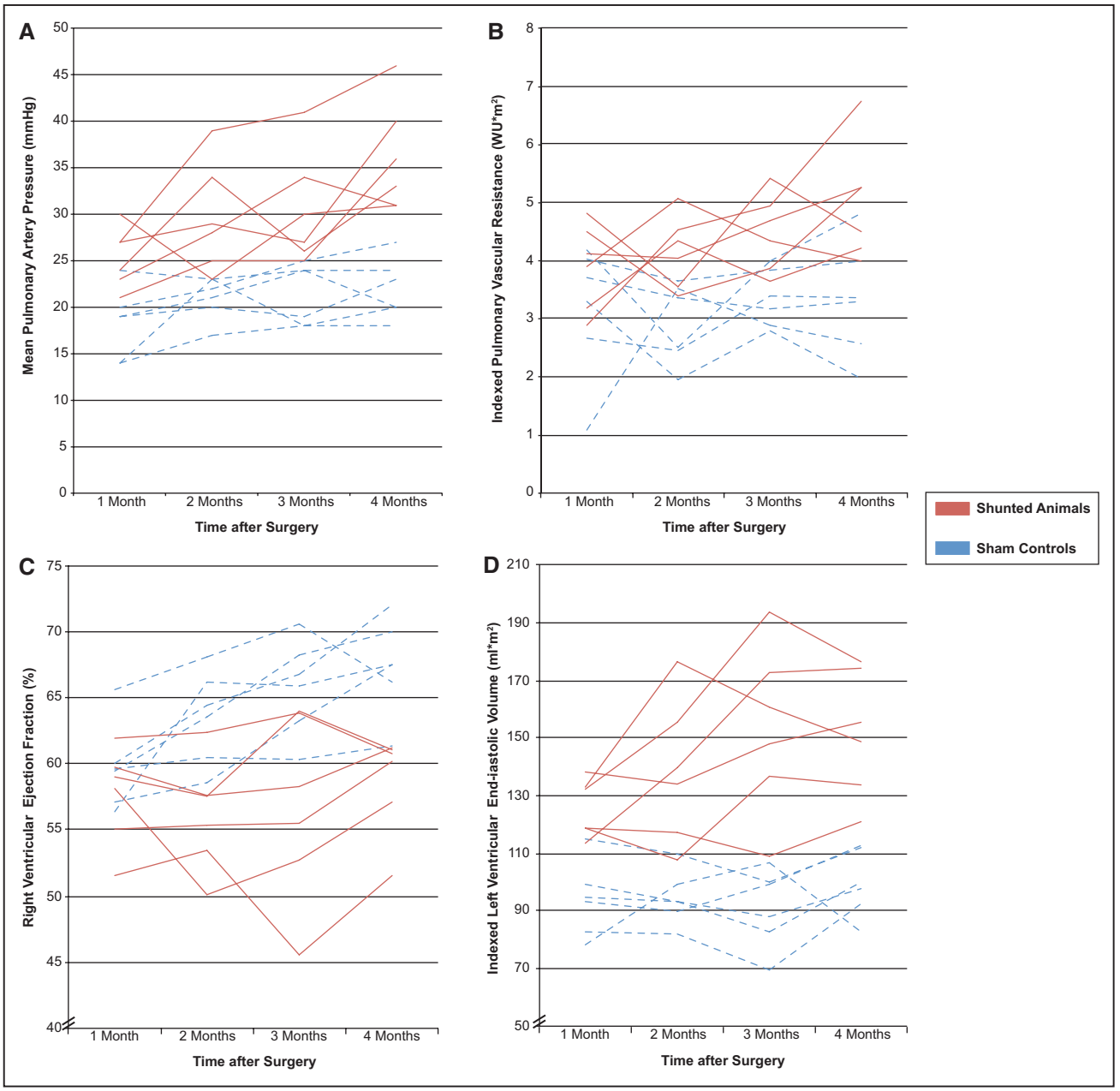

Figure 2. Individual evolution of hemodynamic and CMR parameters in shunted and sham-control cases. Mean pulmonary artery pressure (**A**); indexed pulmonary vascular resistance (**B**); right ventricular ejection fraction (**C**); and end-diastolic left ventricular volume (**D**). CMR indicates cardiac magnetic resonance.

contrast at the great vessels (ICC=0.978, 95% CI 0.943–0.991) or by ventricular volumetry (ICC=0.974, 95% CI 0.923–0.990).

The increase of the flow through the shunt (through-plane phase-contrast acquisition) as the animals grew correlated with the severity of pulmonary hemodynamics and cardiac remodeling (Figure 3). PA average velocity and CMR-estimated PVR using a previously published model[7] correlated with invasive PVR (r=–0.55, P<0.001; and r=0.62, P<0.001).

Cardiac Computed Tomography Data

CT demonstrated patency of the shunt in all cases. Both shunt diameter and cross-sectional area increased during follow-up (Table 2). Shunt area significantly correlated with its flow, as assessed by CMR (r=0.842; P<0.001).

Histopathology Data

Right Ventricle

Animals with aorto-pulmonary shunts showed significant RV hypertrophy macroscopically (Figure 4). Microscopic analysis evidenced significant cardiomyocyte hypertrophy, interstitial fibrosis, marked muscular fiber disarray, and lymphocytic infiltration with collagen deposition around myocardial vessels.

Morphometric quantitative analysis revealed significantly higher connective tissue density in samples from the RV insertion points in shunted animals as compared with controls (38% [38%–42%] versus 22% [19%–25%]; P=0.002). There was a good correlation between collagen content evaluated by histopathology and CMR-estimated ECV (R=0.79; P=0.004).

Table 2. Morphological and Functional Follow-Up Data Obtained by Cardiac Magnetic Resonance and Computed Tomography

	1 Month			2 Months			3 Months			4 Months		
	Shunt (n=6)	Sham (n=6)	*P* Value	Shunt (n=6)	Sham (n=6)	*P* Value	Shunt (n=6)	Sham (n=6)	*P* Value	Shunt (n=6)	Sham (n=6)	*P* Value
CMR parameters												
Indexed RV mass, g/m^2	21.8 (17.7–24.5)	18.6 (15.6–22.6)	0.429	25.8 (19.0–27.4)	19.5 (18.0–20.9)	0.132	22.2 (21.5–23.6)	18.1 (17.8–18.7)	0.015	22.8 (22.6–23.1)	17.5 (16.5–20.9)	0.038
Indexed RVEDV, mL/m^2	81.4 (75.8–83.4)	73.9 (68.4–90.6)	0.931	90.3 (68.4–96.3)	81.4 (75.1–88.1)	0.699	79.4 (77.6–112.33)	74.1 (70.1–92.4)	0.240	82.8 (76.2–84.6)	82.8 (80.5–86.5)	0.792
Indexed RVESV, mL/m^2	34.2 (30.6–35.5)	29.9 (25.5–38.9)	0.537	37.9 (34.1–40.9)	31.3 (24.0–33.1)	0.065	35.3 (28.2–41.2)	25.3 (22.3–30.9)	0.041	32.6 (31.8–33.7)	29.2 (26.1–29.2)	0.030
RVEF, %	58.6 (55.0–59.7)	59.4 (57.1–60.0)	0.537	56.4 (53.4–57.6)	59.8 (55.9–67)	0.009	56.9 (52.7–63.8)	66.4 (63.3–68.2)	0.026	60.4 (57.1–61.0)	67.5 (66.2–70.0)	0.004
Indexed LV mass, g/m^2	53.6 (49.2–57.7)	52.1 (50.0–55.9)	0.792	59.8 (55.9–67.0)	56.0 (46.4–81.8)	0.818	63.2 (59.9–69.6)	56.0 (49.3–61.6)	0.093	66.7 (63.2–70.1)	58.1 (54.5–60.1)	0.052
Indexed LVEDV, mL/m^2	125.6 (118.9–132.7)	94.9 (82.4–99.2)	0.009	137.0 (117.2–155.4)	94.7 (89.0–108.1)	0.004	154.4 (136.9–172.4)	93.5 (82.6–100.0)	0.002	151.8 (133.9–174.5)	97.8 (92.8–112.2)	0.004
Indexed LVESV, mL/m^2	55.8 (52.6–64.0)	43.6 (34.5–46.1)	0.004	60.8 (56.4–71.2)	38.4 (37.1–43.9)	0.002	61.3 (50.8–74.7)	37.5 (32.0–40.5)	0.009	63.8 (58.0–66.6)	38.4 (30.0–40.1)	0.009
LVEF, %	54.4 (51.7–56.0)	56.0 (54.0–57.4)	0.329	54.9 (50.7–56.3)	58.4 (57.6–60.0)	0.026	60.6 (53.5–63.3)	61.7 (59.4–63.0)	0.699	58.2 (56.5–60.3)	65.8 (58.8–67.6)	0.329
E_a/E_{max}	0.38 (0.34–0.48)	0.49 (0.41–0.51)	0.610	0.53 (0.44–0.58)	0.32 (0.28–0.36)	0.009	0.50 (0.37–0.51)	0.29 (0.25–0.37)	0.045	0.40 (0.34–0.57)	0.28 (0.22–0.28)	0.009
Average PA velocity, cm/s	8.6 (7.3–10.0)	15.4 (11.7–17.0)	0.017	8.6 (7.9–9.7)	13.6 (13.2–14.3)	0.015	7.1 (7.0–9.0)	12.8 (11.7–13.8)	0.004	7.7 (6.9–9.4)	11.8 (10.5–12.4)	0.030
Indexed PA area, cm^2/m^2	8.5 (7.7–8.8)	5.9 (5.6–5.9)	0.004	8.4 (7.8–8.4)	6.4 (6.2–6.8)	0.004	8.1 (4.5–8.5)	6.1 (5.5–6.6)	0.009	7.7 (7.5–8.3)	46.3 (5.6–6.7)	0.017
CT parameters												
Shunt area, mm^2	11.5 (10.0–41.0)	NA	NA	81.0 (70.0–153.4)	NA	NA	141.2 (106.0–192.4)	NA	NA	202.5 (135.0–285.8)	NA	NA
Shunt diameter, mm	3.85 (3.7–7.6)	NA	NA	10.8 (10.0–14.5)	NA	NA	13.6 (12.3–15.7)	NA	NA	15.4 (14.2–17.2)	NA	NA

CMR indicates cardiac magnetic resonance; CT, computed tomography; E_a/E_{max}, index of arterial load/index of contractility; LV, left ventricle; LVEDV, left ventricular end-diastolic volume; LVEF, left ventricular ejection fraction; LVESV, left ventricular end-systolic volume; NA, nonapplicable; PA, pulmonary artery; RV, right ventricle; RVEDV, right ventricular end-diastolic volume; RVEF, right ventricular ejection fraction; and RVESV, right ventricular end-systolic volume.

The extracellular fraction was also significantly higher in shunted animals as compared with controls (median values of 36% versus 24%).

Left Ventricle

Macroscopically, LV hypertrophy was observed. Microscopic analysis showed muscular fiber disarray and interstitial

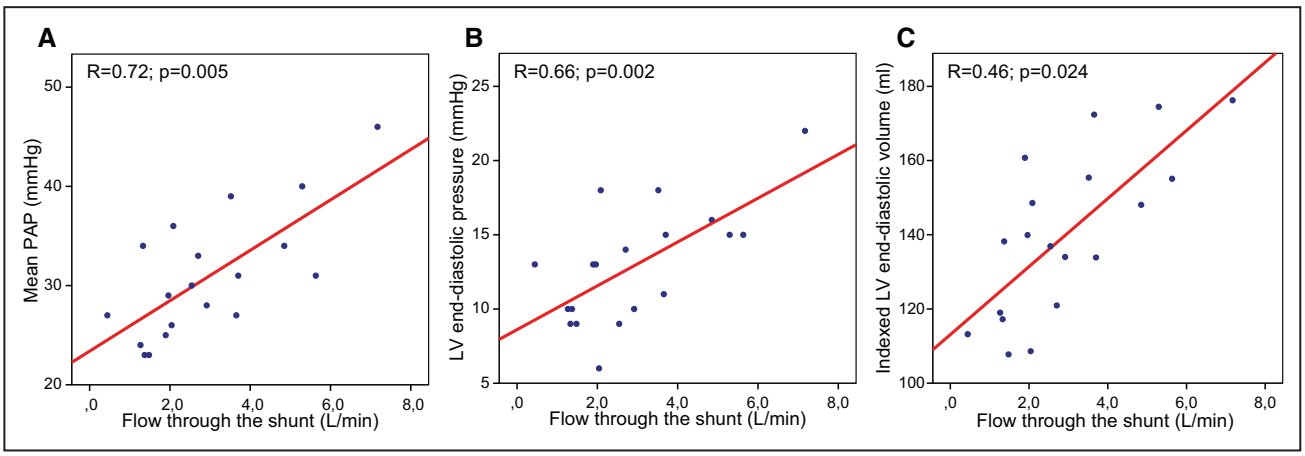

Figure 3. Scatterplot diagrams showing the correlation between the flow through the shunt measured by CMR and mean PAP (**A**), LV end-diastolic pressure (**B**), and indexed LV end-diastolic volume (**C**). CMR indicates cardiac magnetic resonance; LV, left ventricle; and PAP, pulmonary artery pressure.

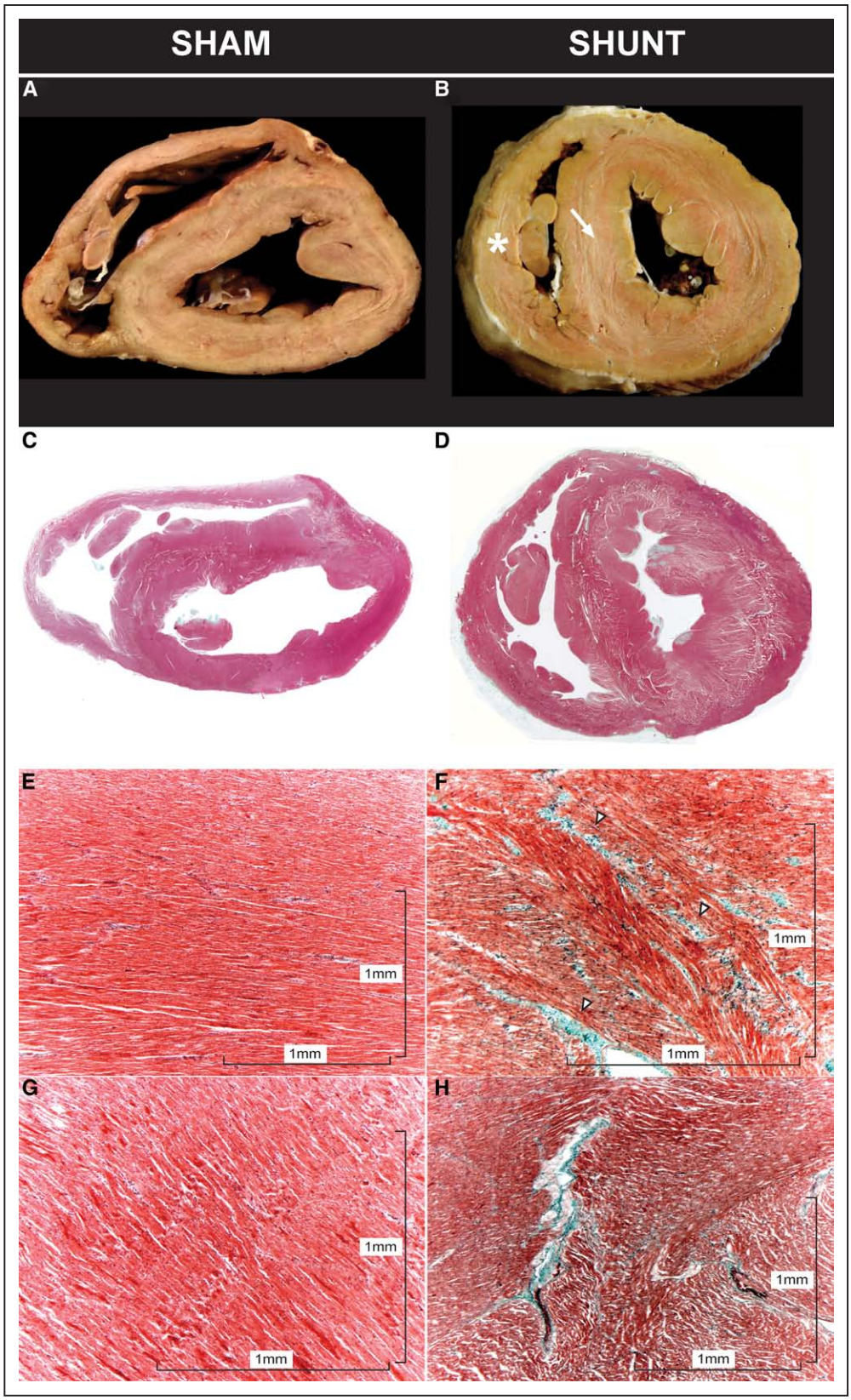

Figure 4. Comparative changes occurring in hearts of animals with aorto-pulmonary shunts (on the right side) compared with controls (on the left side). **A** and **B**, Macroscopic pictures of a cardiac short-axis, midventricular section from a control animal (**A**) and another with aorto-pulmonary shunting (**B**). There is clear biventricular remodeling with marked RV hypertrophy (white asterisk) and septal flattening (white arrow). **C** and **D**, Masson's trichromic staining of the same specimens as shown in A (**C**) and B (**D**), showing myocardial hypertrophy and fiber disarray on both ventricles. **E** and **F**, Microphotographs of RV myocardium from a control (**E**) and an aorto-pulmonary shunt (**F**) using Masson's trichrome staining showing myocardial disarray with marked interstitial fibrosis (white arrowheads). **G** and **H**, Similar preparations as in **E** and **F** but now of the LV from a control (**G**) and an aorto-pulmonary shunt (**H**), also presenting the similar findings as those described on the RV, but comparatively with lesser intensity. LV indicates left ventricle; and RV, right ventricle.

fibrosis, although in a lesser degree than that seen on the RV (Figure 4). Quantitative analysis confirmed significantly higher connective tissue density in the LV lateral wall of shunted animals compared with controls (32.5% [31%–33%] versus 26% [25.5%–27.5%]; *P*=0.024). Similarly, the extracellular fraction in the LV was also significantly higher in shunted animals as compared with controls (median values of 32% versus 29%).

Lung Parenchyma

Arteries inside the lung parenchyma showed increased medial thickening with fiber disarray and increased connective tissue within the media secondary to degeneration and apoptosis of muscular fibers. Endothelial intimal proliferation and fibrosis was evidenced. Significant periadventitial fibrosis and plexiform-like lesions (complex, glomeruloid-like vascular structures originating from the pulmonary arteries) were also observed (Figure 5).

Quantitative analysis from lung samples revealed marked increase in medial thickness (0.14±0.08 mm [range 0.06–0.41 mm] versus controls 0.03±0.01 mm [range 0.01–0.06 mm]) and intimal thickness (0.08±0.02 mm [range 0.02–0.12 mm] versus controls 0.01±0.002 mm [range 0.008–0.02 mm]).

Myocardial ECV Quantified by CMR

For this aim, 20 animals were evaluated 3 months after intervention. One shunted animal was excluded because the shunt was occluded on the CT study. Therefore, 19 animals (9 with aorto-pulmonary shunts and 10 sham controls) were included in this analysis. LGE was not observed in any animal. Intra- and interobserver concordance for T1 and ECV measurements of our laboratory have been described previously.[19]

Compared with sham controls, equilibrium-contrast ECV was significantly higher in shunted animals at the anterior RV insertion point (33.0% [30.4–34.2] versus 25.0% [23.6–26.2]; *P*=0.001), inferior RV insertion point (33.0% [30.6–39.4] versus 24.2% [23.2–25.0]; *P*=0.001), interventricular septum (29.8% [28.2–31.9] versus 24.0% [22.5–28.2]; *P*=0.006), and LV lateral wall (29.3% [28.3–29.9]

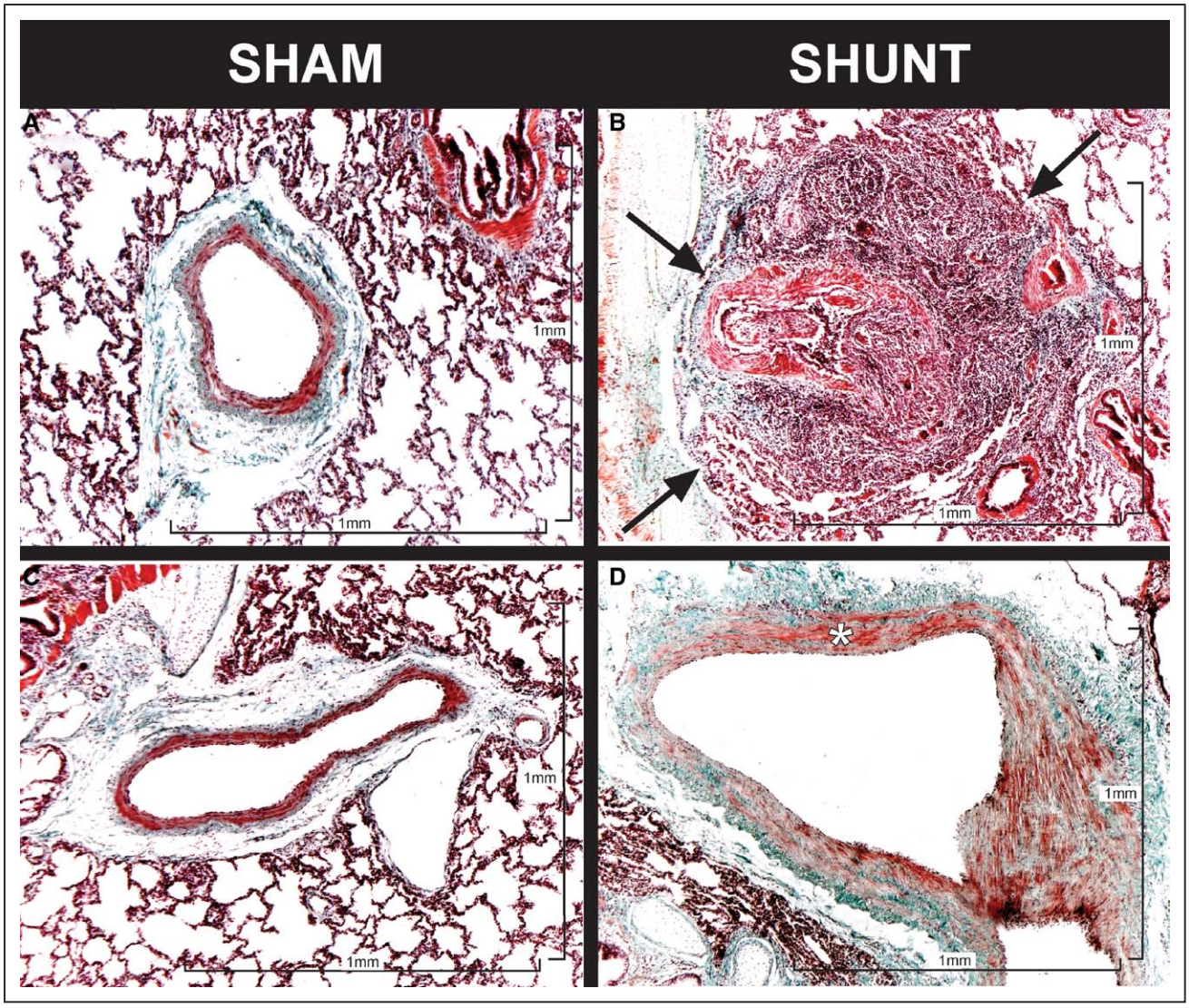

Figure 5. Microphotographs of pulmonary tissue from a sham control (**A** and **C**) and an aorto-pulmonary shunt (**B** and **D**) using Masson's trichrome staining. Animals with aorto-pulmonary shunts presented vascular remodeling inside the lung parenchyma, with marked arterial medial thickening and fibrosis (white asterisk) seen inside the media and intimal layers (**D**). Perivascular fibrosis and plexiform lesions (black arrows) can also be found (**B**).

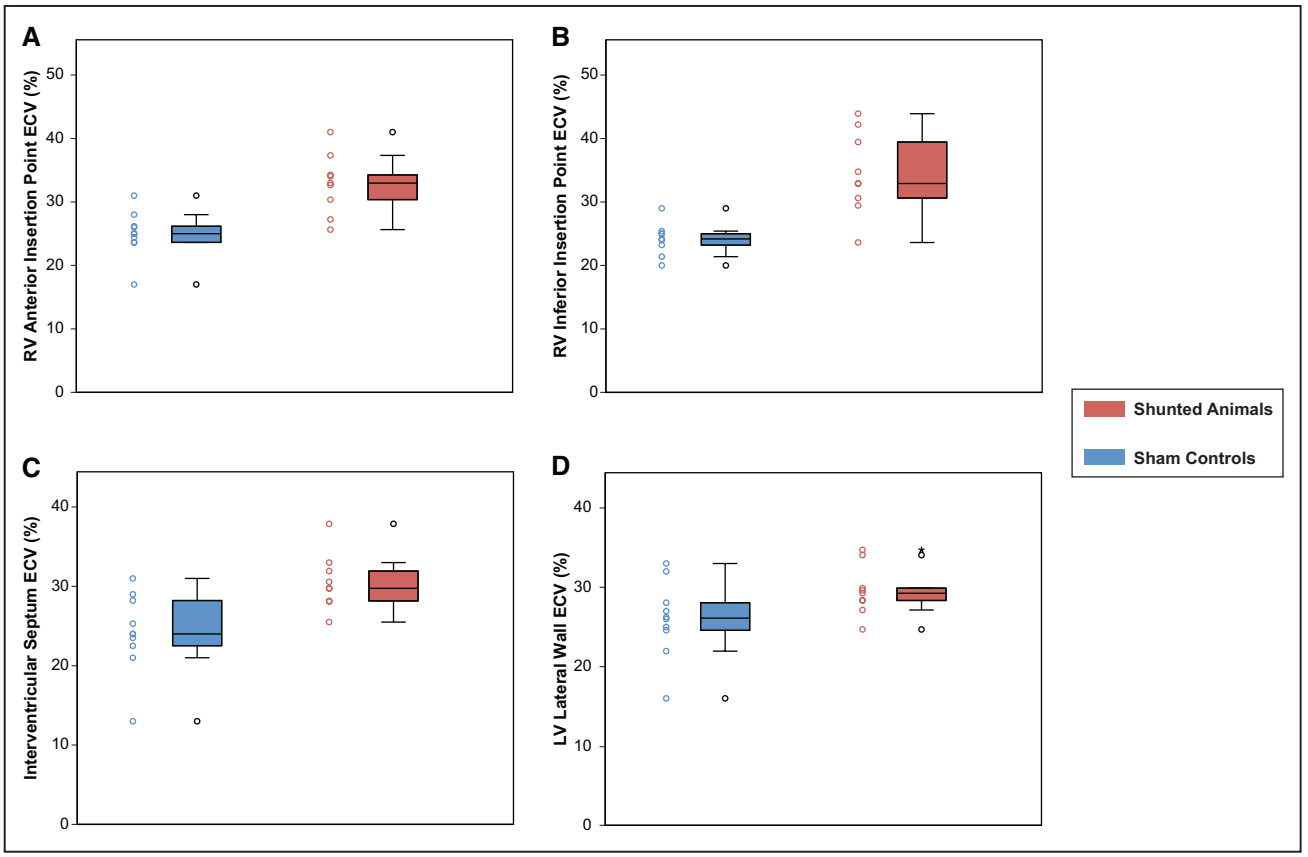

Figure 6. Individual and summarized representation of myocardial ECV values at the 4 different locations in shunted and sham-control animals. Right ventricular anterior insertion point (**A**); right ventricular inferior insertion point (**B**); interventricular septum (**C**); and left ventricular lateral wall (**D**). ECV indicates extracellular volume; LV, left ventricle; and RV, right ventricle.

versus 26.1% [24.6–28.1]; *P*=0.043). Figure 6 shows individual and summarized ECV data at 4 different locations in shunted and control-sham cases.

ECV at the anterior and inferior RV insertion points showed a strong positive correlation with pulmonary hemodynamics and a negative correlation with RV ejection fraction (Figure 7). ECV at both locations correlated also with LV end-diastolic and end-systolic volumes (*r*=0.68, *P*=0.001 and *r*=0.60, *P*=0.006 for the anterior and *r*=0.72, *P*=0.001 and *r*=0.61, *P*=0.008 for the inferior RV insertion point). ECV at the anterior RV insertion point significantly correlated with indexed RV mass (*r*=0.54, *P*=0.016), whereas the correlation did not reach statistical significance for the inferior RV insertion point (*r*=0.45, *P*=0.063). Likewise, ECV at the septum correlated with pulmonary hemodynamics (*r*=0.54, *P*=0.018 for indexed PVR and *r*=0.53, *P*=0.018 for mean PAP). Finally,

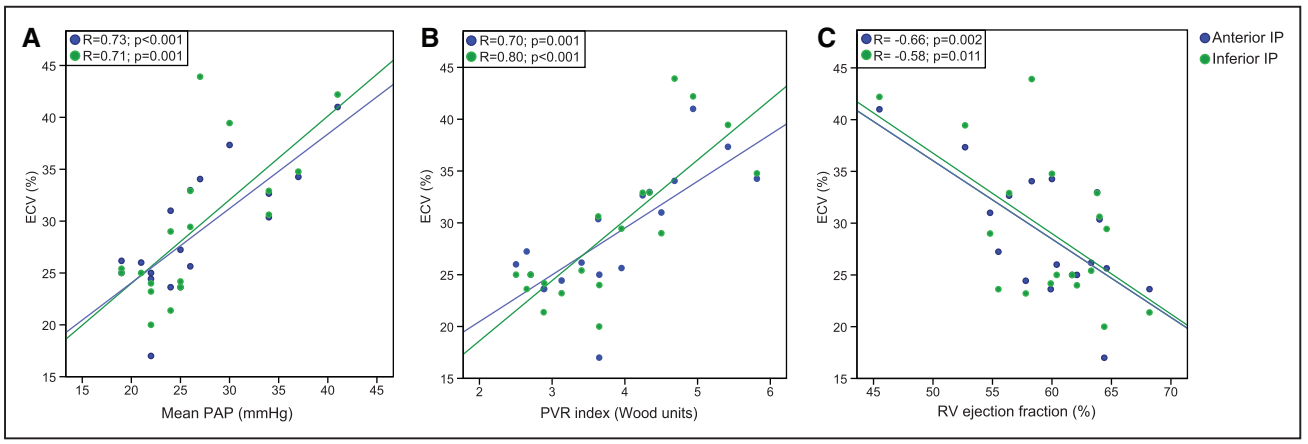

Figure 7. Scatterplot diagrams showing the correlation between the ECV measured by CMR in the anterior (blue dots and line) and posterior (green dots and line) insertion points of the RV and mean PAP (**A**), indexed PVR (**B**), and RV ejection fraction (**C**). CMR indicates cardiac magnetic resonance; ECV, extracellular volume; PAP, pulmonary artery pressure; PVR, pulmonary vascular resistance; and RV, right ventricle.

ECV at the LV lateral wall correlated with pulmonary hemodynamics (r=0.52, P=0.022 for indexed PVR and r=0.47, P=0.041 for mean PAP) and LV end-diastolic and end-systolic volumes (r=0.47, P=0.044 and r=0.53, P=0.020).

Native precontrast T1 values at the anterior RV insertion point, the inferior RV insertion point, the septum, and the LV lateral wall were higher in shunted animals than in controls, although differences did not reach statistical significance (1042 [1009–1044] ms versus 981 [958–1027] ms, P=0.113; 1013 [976–1050] ms versus 967 [963–997] ms, P=0.190; 1024 [1007–1059] ms versus 954 [922–1029] ms, P=0.243; and 1003 [948–1073] versus 976 [936–1078] ms, P=0.661, respectively). At the time CMR was performed, heart rate was not statistically different between shunted and sham animals (88 [82–94] ppm versus 79.5 [70–88], respectively; P=0.18), and there was no correlation between heart rate and T1 and ECV measurements (P value >0.5 in all cases).

Discussion

The present study shows that prolonged systemic-to-pulmonary shunting in growing piglets induces biventricular remodeling and myocardial fibrosis that can be detected and monitored using CMR. The main results of the study are the following: (1) T1-mapping sequences on CMR demonstrate increased ECV at the RV insertion points, the interventricular septum, and the LV lateral wall, reproducing the pattern of fibrosis found on pathology in a noninvasive manner; (2) ECV at the RV insertion points strongly correlates with pulmonary hemodynamics and RV systolic function; (3) CMR imaging evidences progressive RV hypertrophy and dysfunction and LV severe dilatation; (4) CO quantified by CMR shows an excellent correlation with CO measured by RHC; (5) flow through the shunt quantified by CMR strongly correlates with the severity of PH, LVEDP, and LV dilatation.

The original model of left-to-right shunt-induced PH in piglets, proposed by Rendas et al[22] in 1979, used a prosthetic graft between the PA and the descending aorta, but achieved only a modest increase in PAP. Rondelet et al[13] and Wauthy et al[15] introduced a modification by anastomosing the left innominate artery to the PA, thus, allowing for progressive increase in shunt size. Both authors reported a moderate increase in systolic PAP after 10 to 12 weeks with arterial medial hypertrophy but not other characteristics of PH. Rondelet et al[16] recently reported the hemodynamic and pathobiological data at 6 months after shunt closure. Prolonged shunting resulted in a modest increase in mean PAP and PVR with a significant decrease in E_{es}/E_a ratio evaluated by RV pressure–volume loops and cardiac index. Increased medial thickness in the lung parenchyma and biventricular cardiomyocyte hypertrophy with interstitial fibrosis was found in pathology. They did not perform serial evaluations and, other than data from RV pressure–volume loops, did not describe cardiac remodeling and performance. Also importantly, they did not report the significant changes occurring in the LV we have seen in our study (eg, LV dilatation, interstitial fibrosis, fiber disarray, and increased filling pressures) that are also typically found in patients with CHD similar to our model, like a patent ductus arteriosus.

In the present study, besides serial hemodynamic evaluation and pathology description, we performed a comprehensive characterization of structural cardiac changes that occurred because of pulmonary overcirculation using CMR. We have been able to demonstrate that this model reproduces biventricular remodeling as that observed in patients with left-to-right shunts and proves as an excellent tool to evaluate diagnostic or therapeutic strategies. Significant differences were observed in RV ejection fraction and LV dimensions between shunt cases and sham controls from the second month. In controls, a progressive increase in RV ejection fraction during the study was observed. This may be related with the physiological change in cardiac chamber dimensions and contractility with growth, and it has also been observed in other studies with the same pig breed[23]; however, this increase in RV ejection fraction was not observed in shunted animals. Hemodynamic findings resembled those previously described, but considerably higher differences between controls and shunted animals were observed. PVR in both shunted and control cases was higher at the first month than later on. The early fall in PVR correlates with the RV ejection fraction finding and might be because of different factors. First, animal growth in the third and four month after birth is fast, and consequently, the increase in lung size and lung vasculature is important and partially compensates the increase in CO. When PVR is indexed by body surface area, this fall is no longer observed. Second, in the adaptation of the RV to PH, it is known that there is an initial increase in RV contractility, which explains why ventriculoarterial coupling is relatively maintained in earlier stages.[24] Indeed, in our study, estimated E_a/E_{max} in shunt cases remained relatively stable during follow-up. Both LVEDP and transpulmonary gradient increased during follow-up. The increase in the transpulmonary gradient may be related with the fact that both shunt diameter and flow increased greatly during the study, as opposed to what is seen in patients with prosthetic shunts for palliation of cyanotic heart disease.

As a reflection of more severe PH generated in our model, we observed not only medial hypertrophy but also significant intimal hypertrophy and fibrosis and plexiform-like lesions in the lung parenchyma, typical features of advanced PH. The development of a more severe disease, including histological changes, as compared with previous studies by Wauthy et al and Rondelet et al might partially have been the consequence of using a different pig breed, with greater increase in body weight and shunt growth. Another possible explanation is that, unlike in previous studies, we confirmed by cardiac CT that the shunt was patent in all animals before all follow-up studies. Closure of the shunt before hemodynamic assessment might have partially reduced the severity of PH; we decided to maintain the shunt patent to allow us to make serial evaluations and to reproduce the uncorrected CHD with pulmonary overcirculation scenario as reliably as possible.

We demonstrate that CMR is able to quantify not only macroscopic cardiac changes but also microstructural involvement in a noninvasive way. CMR allowed detection of myocardial ECV expansion that affected the RV insertion points, the interventricular septum, and the LV lateral wall 3 months after intervention. We decided to use this time point to allow comparisons with previous studies using this model because, according to these previous studies, this time was compatible with early PH. Indeed, LGE was not observed in any animal,

and RV ejection fraction could be considered as preserved at this time point (median of 57%), although it was reduced as compared with controls. In an experimental model of post-capillary PH induced by pulmonary vein banding, CMR-measured ECV at the RV insertion points was significantly higher in banded animals than in controls and showed significant correlation with pulmonary hemodynamics and RV performance.[19] In this previous study, only a nonsignificant trend toward higher ECV at the septum and LV lateral wall was observed.[25] In the current model, ECV was again significantly higher at the RV insertion points, showing a good correlation with the severity of PH, but differences in ECV at the septum and LV lateral wall were also significant, reflecting an inherent damage at the LV. Pressure overload and, remarkably, significant lung parenchymal damage[26] seem to induce greater myocardial fibrosis than volume overload. At the time LVEDP reached a clinically significant increase in shunted cases, a significant ECV expansion was already present. Native pre-contrast T1 values were higher in all territories in shunted animals, although differences did not reach statistical significance, confirming previous data regarding the superiority of ECV over native T1 value for early detection of myocardial damage. Unlike native T1, ECV requires gadolinium administration. Nevertheless, gadolinium is commonly administered in CHD patients, and the incidence of adverse effects related to its use is low.[27,28] In addition, gadolinium administration allows detection of macroscopic myocardial fibrosis or scarring (LGE), which is considered irreversible and associated with advanced stages of the disease.

The present study may have the following clinical implications: myocardial fibrosis seems to appear very early after aorto-pulmonary shunting, becoming a potential early marker of biventricular remodeling and RV dysfunction; evaluation of diffuse fibrosis by CMR in the setting of pulmonary overcirculation may become a useful tool in the management of patients with CHD; finally, this translational experimental model has the potential to allow the evaluation of new diagnostic tools and therapeutic strategies in this scenario.

Some study limitations should be acknowledged. T1-mapping sequences were only performed in a single time point for all cases, precluding the evaluation of temporal relationships between hemodynamics and the onset of myocardial fibrosis on CMR. Because of the number of comparisons performed and limited sample sizes, a risk for type I error should be acknowledged. Longer follow-up would be necessary to confirm that ECV expansion identifies patients at risk of developing RV failure and its reversibility after surgery. Also, longer follow-up might allow us to see relevant changes in transpulmonary gradient, ventriculo-arterial coupling, and RV dysfunction. In this sense, we are planning to characterize the same model in minipigs whose longer follow-up is not restricted by the accelerated animal growth. Clinical validation in patients with PH because of overcirculation should be performed in the future.

In conclusion, this is the first study that focuses specifically on characterizing biventricular performance and the noninvasive detection of early myocardial fibrosis in a model of aorto-pulmonary shunt. These results may prove useful in the future for monitoring patients with CHD and left-to-right shunting.

Sources of Funding

This work was supported by a competitive grant from the Spanish Ministry of Economy and Competitiveness (MINECO) through the Carlos III Institute of Health-Fondo de Investigación Sanitaria and European Regional Development Fund (ERDF/FEDER) funds (PI13/02339 to Dr García-Álvarez) and by the competitive grant CNIC-Translational 01-2009 (to Dr Ibáñez). Other sponsors were a grant TIN2012–37546-C03-02 from the Ministerio de Economía y Competitividad (to Dr Sánchez-Quintana), a FPU program (13/02662) from the Ministerio de Educación, Cultura y Deporte (to F. Sierra) and a Master Research Agreement (MRA) between Philips healthcare and CNIC. Drs García-Álvarez and Ibáñez are members of the Spanish "Red de Investigación Cardiovascular" (RIC, RD 12/0042/0054). The CNIC is supported by the Spanish Ministry of Economy and Competitiveness (MINECO) and the Pro-CNIC Foundation and is a Severo Ochoa Center of Excellence (MINECO award SEV-2015-0505).

Disclosures

None.

References

1. Engelfriet PM, Duffels MG, Möller T, Boersma E, Tijssen JG, Thaulow E, Gatzoulis MA, Mulder BJ. Pulmonary arterial hypertension in adults born with a heart septal defect: the Euro Heart Survey on adult congenital heart disease. *Heart*. 2007;93:682–687. doi: 10.1136/hrt.2006.098848.
2. Simonneau G, Gatzoulis MA, Adatia I, Celermajer D, Denton C, Ghofrani A, Gomez Sanchez MA, Krishna Kumar R, Landzberg M, Machado RF, Olschewski H, Robbins IM, Souza R. Updated clinical classification of pulmonary hypertension. *J Am Coll Cardiol*. 2013;62(25 suppl):D34–D41. doi: 10.1016/j.jacc.2013.10.029.
3. Lowe BS, Therrien J, Ionescu-Ittu R, Pilote L, Martucci G, Marelli AJ. Diagnosis of pulmonary hypertension in the congenital heart disease adult population impact on outcomes. *J Am Coll Cardiol*. 2011;58:538–546. doi: 10.1016/j.jacc.2011.03.033.
4. Norozi K, Wessel A, Alpers V, Arnhold JO, Geyer S, Zoege M, Buchhorn R. Incidence and risk distribution of heart failure in adolescents and adults with congenital heart disease after cardiac surgery. *Am J Cardiol*. 2006;97:1238–1243. doi: 10.1016/j.amjcard.2005.10.065.
5. Carmosino MJ, Friesen RH, Doran A, Ivy DD. Perioperative complications in children with pulmonary hypertension undergoing noncardiac surgery or cardiac catheterization. *Anesth Analg*. 2007;104:521–527. doi: 10.1213/01.ane.0000255732.16057.1c.
6. García-Álvarez A, Fernández-Friera L, García-Ruiz JM, Nuño-Ayala M, Pereda D, Fernández-Jiménez R, Guzmán G, Sanchez-Quintana D, Alberich-Bayarri A, Pastor-Escuredo D, Sanz-Rosa D, García-Prieto J, Gonzalez-Mirelis JG, Pizarro G, Jimenez-Borreguero LJ, Fuster V, Sanz J, Ibáñez B. Noninvasive monitoring of serial changes in pulmonary vascular resistance and acute vasodilator testing using cardiac magnetic resonance. *J Am Coll Cardiol*. 2013;62:1621–1631. doi: 10.1016/j.jacc.2013.07.037.
7. García-Alvarez A, Fernández-Friera L, Mirelis JG, Sawit S, Nair A, Kallman J, Fuster V, Sanz J. Non-invasive estimation of pulmonary vascular resistance with cardiac magnetic resonance. *Eur Heart J*. 2011;32:2438–2445. doi: 10.1093/eurheartj/ehr173.
8. Babu-Narayan SV, Goktekin O, Moon JC, Broberg CS, Pantely GA, Pennell DJ, Gatzoulis MA, Kilner PJ. Late gadolinium enhancement cardiovascular magnetic resonance of the systemic right ventricle in adults with previous atrial redirection surgery for transposition of the great arteries. *Circulation*. 2005;111:2091–2098. doi: 10.1161/01.CIR.0000162463.61626.3B.
9. Oosterhof T, Mulder BJ, Vliegen HW, de Roos A. Corrected tetralogy of Fallot: delayed enhancement in right ventricular outflow tract. *Radiology*. 2005;237:868–871. doi: 10.1148/radiol.2373041324.
10. Wald RM, Haber I, Wald R, Valente AM, Powell AJ, Geva T. Effects of regional dysfunction and late gadolinium enhancement on global right ventricular function and exercise capacity in patients with repaired tetralogy of Fallot. *Circulation*. 2009;119:1370–1377. doi: 10.1161/CIRCULATIONAHA.108.816546.

11. Kramer CM, Chandrashekhar Y, Narula J. T1 mapping by CMR in cardiomyopathy: a noninvasive myocardial biopsy? *JACC Cardiovasc Imaging*. 2013;6:532–534. doi: 10.1016/j.jcmg.2013.02.002.
12. Riesenkampff E, Messroghli DR, Redington AN, Grosse-Wortmann L. Myocardial T1 mapping in pediatric and congenital heart disease. *Circ Cardiovasc Imaging*. 2015;8:e002504. doi: 10.1161/CIRCIMAGING.114.002504.
13. Rondelet B, Kerbaul F, Motte S, van Beneden R, Remmelink M, Brimioulle S, McEntee K, Wauthy P, Salmon I, Ketelslegers JM, Naeije R. Bosentan for the prevention of overcirculation-induced experimental pulmonary arterial hypertension. *Circulation*. 2003;107:1329–1335.
14. Rondelet B, Kerbaul F, Van Beneden R, Motte S, Fesler P, Hubloue I, Remmelink M, Brimioulle S, Salmon I, Ketelslegers JM, Naeije R. Signaling molecules in overcirculation-induced pulmonary hypertension in piglets: effects of sildenafil therapy. *Circulation*. 2004;110:2220–2225. doi: 10.1161/01.CIR.0000143836.40431.F5.
15. Wauthy P, Abdel Kafi S, Mooi WJ, Naeije R, Brimioulle S. Inhaled nitric oxide versus prostacyclin in chronic shunt-induced pulmonary hypertension. *J Thorac Cardiovasc Surg*. 2003;126:1434–1441. doi: 10.1016/S0022.
16. Rondelet B, Dewachter C, Kerbaul F, Kang X, Fesler P, Brimioulle S, Naeije R, Dewachter L. Prolonged overcirculation-induced pulmonary arterial hypertension as a cause of right ventricular failure. *Eur Heart J*. 2012;33:1017–1026. doi: 10.1093/eurheartj/ehr111.
17. Brody S. A comparison of growth curves of man and other animals. *Science*. 1928;67:43–46.
18. Fratz S, Chung T, Greil GF, Samyn MM, Taylor AM, Valsangiacomo Buechel ER, Yoo SJ, Powell AJ. Guidelines and protocols for cardiovascular magnetic resonance in children and adults with congenital heart disease: SCMR expert consensus group on congenital heart disease. *J Cardiovasc Magn Reson*. 2013;15:51. doi: 10.1186/1532-429X-15-51.
19. García-Álvarez A, García-Lunar I, Pereda D, Fernández-Jimenez R, Sánchez-González J, Mirelis JG, Nuño-Ayala M, Sánchez-Quintana D, Fernández-Friera L, García-Ruiz JM, Pizarro G, Agüero J, Campelos P, Castellá M, Sabaté M, Fuster V, Sanz J, Ibañez B. Association of myocardial T1-mapping CMR with hemodynamics and RV performance in pulmonary hypertension. *JACC Cardiovasc Imaging*. 2015;8:76–82. doi: 10.1016/j.jcmg.2014.08.012.
20. Sanz J, García-Alvarez A, Fernández-Friera L, Nair A, Mirelis JG, Sawit ST, Pinney S, Fuster V. Right ventriculo-arterial coupling in pulmonary hypertension: a magnetic resonance study. *Heart*. 2012;98:238–243. doi: 10.1136/heartjnl-2011-300462.
21. Flett AS, Hayward MP, Ashworth MT, Hansen MS, Taylor AM, Elliott PM, McGregor C, Moon JC. Equilibrium contrast cardiovascular magnetic resonance for the measurement of diffuse myocardial fibrosis: preliminary validation in humans. *Circulation*. 2010;122:138–144. doi: 10.1161/CIRCULATIONAHA.109.930636.
22. Rendas A, Lennox S, Reid L. Aorta-pulmonary shunts in growing pigs. Functional and structural assessment of the changes in the pulmonary circulation. *J Thorac Cardiovasc Surg*. 1979;77:109–118.
23. Pereda D, García-Alvarez A, Sánchez-Quintana D, Nuño M, Fernández-Friera L, Fernández-Jiménez R, García-Ruíz JM, Sandoval E, Aguero J, Castellá M, Hajjar RJ, Fuster V, Ibáñez B. Swine model of chronic postcapillary pulmonary hypertension with right ventricular remodeling: long-term characterization by cardiac catheterization, magnetic resonance, and pathology. *J Cardiovasc Transl Res*. 2014;7:494–506. doi: 10.1007/s12265-014-9564-6.
24. Chantler PD, Melenovsky V, Schulman SP, Gerstenblith G, Becker LC, Ferrucci L, Fleg JL, Lakatta EG, Najjar SS. The sex-specific impact of systolic hypertension and systolic blood pressure on arterial-ventricular coupling at rest and during exercise. *Am J Physiol Heart Circ Physiol*. 2008;295:H145–H153. doi: 10.1152/ajpheart.01179.2007.
25. Usui S, Yao A, Hatano M, Kohmoto O, Takahashi T, Nagai R, Kinugawa K. Upregulated neurohumoral factors are associated with left ventricular remodeling and poor prognosis in rats with monocrotaline-induced pulmonary arterial hypertension. *Circ J*. 2006;70:1208–1215.
26. Bogaard HJ, Natarajan R, Henderson SC, Long CS, Kraskauskas D, Smithson L, Ockaili R, McCord JM, Voelkel NF. Chronic pulmonary artery pressure elevation is insufficient to explain right heart failure. *Circulation*. 2009;120:1951–1960. doi: 10.1161/CIRCULATIONAHA.109.883843.
27. Dorfman AL, Odegard KC, Powell AJ, Laussen PC, Geva T. Risk factors for adverse events during cardiovascular magnetic resonance in congenital heart disease. *J Cardiovasc Magn Reson*. 2007;9:793–798. doi: 10.1080/10976640701545305.
28. Dillman JR, Ellis JH, Cohan RH, Strouse PJ, Jan SC. Frequency and severity of acute allergic-like reactions to gadolinium-containing i.v. contrast media in children and adults. *AJR Am J Roentgenol*. 2007;189:1533–1538. doi: 10.2214/AJR.07.2554.

CLINICAL PERSPECTIVE

Pulmonary hypertension and right ventricular dysfunction are strong predictors of morbidity and mortality among patients with congenital heart disease. Early detection of right ventricular involvement may be useful in the management of these patients, and translational experimental models may advance our knowledge in this field. Cardiac magnetic resonance is a noninvasive diagnostic tool that allows accurate evaluation of biventricular remodeling and function without the use of radiation. The addition of new T1-mapping sequences also allows cardiac magnetic resonance to detect incipient diffuse fibrosis of the ventricular myocardium. Our model of systemic-to-pulmonary shunting produces significant pulmonary hypertension with biventricular remodeling and reproduces all the typical histological features of advanced pulmonary hypertension on the heart and lungs. We have been able to describe and quantify the development of diffuse fibrosis by measuring extracellular volume using cardiac magnetic resonance and also found that diffuse fibrosis in the insertion points of the right ventricle in the interventricular septum correlates with the severity of pulmonary hypertension and right ventricular dysfunction. Fibrosis appears early in systemic-to-pulmonary shunt, becoming a potential early marker of biventricular impairment. These results may prove useful for the early diagnosis of cardiac impairment in patients with pulmonary overcirculation and have the potential to improve the monitoring and management of this group of patients in the future.